J Mater Sci (2007) 42:4334–4343
DOI 10.1007/s10853-006-0686-3

Martensite/particle interactions and the shape memory effect in an Fe–Mn–Si-based alloy

Nicole Stanford · Druce P. Dunne

Received: 20 December 2005 / Accepted: 19 July 2006 / Published online: 28 February 2007

Abstract The effect of carbide precipitates with a size range of 30–300 nm on the austenite to martensite transformation has been studied. Such particles are known to enhance shape memory, and it was the aim of this work to clarify how the particles exert a favourable effect on shape memory. Differential scanning calorimetry revealed that the presence of particles increases the amount of thermally induced martensite. X-ray diffraction showed that the presence of particles increases the amount of stress-induced martensite also. Surface-relief produced on a pre-polished surface by bending deformation showed that the particle-containing samples exhibited a more complex and highly tilted surface-relief indicative of the formation of a larger volume fraction of martensite. The reversion characteristics of the particle-containing and solution-treated samples were similar: both showed co-reversion of multiple variants of martensite within the same volume of microstructure. However, a higher volume fraction of martensite reverted for the particle-containing sample on recovery annealing. The increased density of nucleation sites for martensite formation and a higher volume fraction of stress-induced martensite for a given strain are therefore considered to be the main contributions of relatively coarse carbide particles to the improvement of shape memory performance.

N. Stanford (✉) · D. P. Dunne
Faculty of Engineering, University of Wollongong,
Northfields Ave., Wollongong 2522, Australia
e-mail: stanford@uow.edu.au

Introduction

It has recently been shown that precipitation of NbC in the austenite phase increases the shape memory effect (SME) in Fe–Mn–Si-based alloys [1–3]. Kajiwara et al. [1] proposed that the effect of the precipitates is possibly threefold: precipitates are preferential sites for nucleation of martensite; they strengthen the austenite and therefore inhibit deformation by slip; and thirdly they provide a back-stress for martensite reversion. All these mechanisms are plausible, and there are more possible advantages (and disadvantages) of carbide precipitation that have not been discussed extensively in open literature. For example, SME could be influenced by removal of interstitial carbon from the parent phase, limiting the width and length of martensite plates, or changing the proportion of different variants formed during deformation.

Although there is an extensive array of transmission electron micrographs (TEM) in the literature of NbC particles in austenitic Fe–Mn–Si-based alloys, there is little understanding of how precipitates affect either martensite formation or its reversion. It was therefore the aim of the work described in this paper to achieve greater insight into the mechanisms of martensite formation and reversion in an iron-based shape memory alloy containing second phase particles. To eliminate variables, the alloy was not trained or rolled after solution treatment. It was solution treated, with and without a subsequent isothermal heat treatment to produce particles. Therefore any increase in shape memory is expected to be due to precipitation alone. Instead of NbC precipitate, TiC was the precipitate species investigated in the current study because the SME has been found

to be slightly better for this particular precipitate than for NbC [4].

Experimental methods

The stainless alloy used in this study was made by arc melting of a 27 g button. The composition of the alloy is detailed in Table 1. The as-cast alloy was hot rolled at 900 °C to a thickness of ~1 mm. The rolled strip was sectioned and solution treated at 1,100 °C for 1 h under a flowing argon atmosphere, followed by a cold water quench. Samples in this condition are referred to in the text as ''solution-treated''. After solution treatment, samples were precipitation heat treated at 800 °C for 15 min. In previous work [4] this treatment was found to produce TiC precipitates in the range of 30–300 nm in diameter, with an average diameter of 220 nm. Samples in this condition are referred to as ''particle-containing''.

The shape memory effect (SME) was measured using bend tests with pre-strains between 1% and 6% and a sample thickness of 960 μm. A range of pre-strains was accomplished by bending samples around different rods of different radii. The pre-strain was taken as the maximum tensile/compressive strain, and is determined by the equation:

$$\varepsilon = \frac{1}{(2R/h)+1} \quad (1)$$

where ε = conventional strain, R = bend radius and h = sample thickness.

The shape was recovered by annealing in a muffle furnace at 250 °C for 15 min. After the samples had been recovery annealed the residual strain (ε_r) due to incomplete recovery was calculated using Eq. 1. The percentage recovery was determined by the equation:

$$\%\,\text{recovery} = (\varepsilon - \varepsilon_r)/\varepsilon\,(\times 100\%) \quad (2)$$

The microstructure was investigated in two ways; by surface-relief and by conventional optical microscopy. The surface-relief observations were made on the longitudinal transverse face of strip shaped bend specimens. This transverse face is not in contact with the die during deformation, and has an outer tensile edge and an inner compressive edge that develop during bending. There is a linear strain gradient from zero in the centre to the maximum tensile/compressive strain at the outer edge as calculated using Eq. 1. The surface-relief produced by deformation was observed by firstly pre-polishing the transverse face of the specimen, and then subjecting the sample to the bending strain. The surface-relief was photographed using standard bright field optical microscopy, and was also investigated using atomic force microscopy (AFM). The AFM data were acquired in ''contact'' mode on a Digital Instruments Dimensions 3100 with version 5.12 software.

To investigate the surface-relief produced by reversion of martensite to austenite, specimens were deformed by bending, polished on the transverse face and then recovery annealed. The surface-relief produced is the result of the reversion process, and the surface topography of these specimens was examined by optical microscopy and AFM.

For standard optical microscopical examination, the bend test specimens were mounted and polished using standard metallographic techniques. For both types of samples: surface-relief and optical microstructure, the surface deformation produced by mechanical polishing was removed by a final polish with colloidal silica (Struers OPS) for 10 min. For optical microscopy these samples were then etched in acid ferric chloride to reveal the microstructure.

Microstructural examination of samples was also carried out by transmission electron microscopy (TEM). For this analysis, particle-containing samples were cold rolled to a strain of 5% reduction, and 3 mm discs were spark cut from the rolled sheet. After grinding to 100 μm thickness, the TEM foils were made using a Tenupol jet-polisher with a solution of 5% perchloric acid in acetic acid at 30 V. TEM observations were made using a JEOL JEM 2010 TEM. The transformation behaviour of the samples was investigated using a TA Q100 differential scanning calorimeter (DSC) at a scan rate of 10 °C/min. X-ray diffraction was carried out on a Philips 1730 X-ray generator with Cu Kα radiation.

Table 1 Alloy composition in weight percentage measured using energy dispersive spectroscopy

C[a]	Mn	Si	Ni	Cr	Fe	Ti
0.06	12.5	4.5	6.2	9.4	Balance	0.5

[a] Carbon measured using spectrographic analysis

Results

Transformation and shape memory behaviour

The shape recovery of the solution-treated and particle-containing samples, tested in bending, is shown in Fig. 1. As can be seen, the SME of the

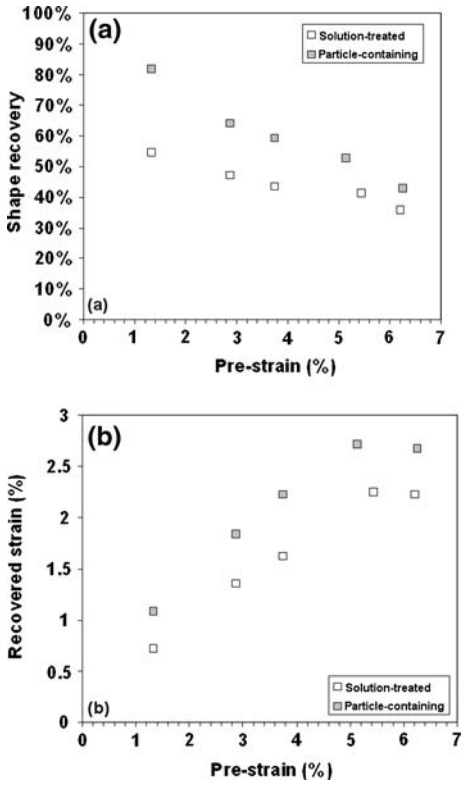

Fig. 1 Shape memory of solution-treated and particle-containing samples measured in bending. (**a**) % Strain recovery, (**b**) recovered strain (%)

particle-containing samples was consistently higher than for the solution treated condition. The maximum recovered strain occurred for a pre-strain of about 5%, and was 2.7% after the precipitation treatment, compared with 2.2% in the solution-treated condition. The Vickers hardness of samples was virtually unchanged by heat treatment, being ~200 HV in both samples.

The transformation behaviour was investigated by DSC. Before measurement, samples of 25–40 mg in mass were immersed in liquid nitrogen to induce thermal transformation to martensite. The samples were then heated from room temperature to 300 °C at 10 °C/min. The DSC results from the solution-treated and particle-containing samples are shown in Fig. 2. The transformation temperatures were not significantly affected by the precipitation treatment. However, the heat of formation was significantly larger in the particle-containing sample. The martensite start temperature was below the temperature limit of the DSC used which is –50 °C.

The amount of martensite present in the specimens was also examined using X-ray diffraction (XRD). For this analysis, samples of the solution-treated and particle-containing alloys were cold rolled to a reduction of 5% strain. The XRD spectrum for each sample was measured between 2θ angles of 45° and 52°. This range encompasses the $(10\bar{1}0)$ ε martensite peak and the (200) γ austenite peak. The number of counts in each martensite and austenite peak were recorded, and then the ratio of martensite counts to the total counts determined. This provided a measure of the amount of martensite present, and the higher the ratio of $\varepsilon/(\varepsilon + \gamma)$, the larger the volume fraction of martensite. The results of this analysis are shown in Fig. 3. There was only a small difference between the amount of martensite present in the two samples, however, the results do indicate that there is more martensite present in the particle-containing compared to the solution-treated sample. These same samples were then recovery annealed at 250 °C, and the XRD measurements repeated (Fig. 3). These measurements show that after recovery, the particle-containing alloy contains slightly less martensite, compared to the solution-treated sample.

Microstructure and surface-relief from deformation

A group of samples was polished flat on the transverse face and then deformed by bending to approximately 5% strain. The surface-relief induced by bending was photographed (Fig. 4). The surface-relief was inhomogeneous—it exhibited some regions containing highly tilted surfaces, regions with no surface tilt, and also regions of clearly defined martensite plates. The latter areas of well defined martensite plates often reflected the size and shape of the parent austenite grains. As has been observed previously [5], the tensile edges showed more extensive surface tilting compared with the compressive regions. The compressive regions had a more rumpled appearance in both samples. Although the bending-induced surface-relief was basically similar for both the particle-containing and solution-treated samples, the particle-containing sample exhibited more severe surface tilting for the highest tensile strains on the outer edges of the sample, and was typically more complex in appearance compared to the solution-treated sample (see, for example, the arrowed region in Fig. 4).

The surface-relief induced by deformation was further investigated using AFM (Fig. 5). AFM showed that some regions exhibited finely spaced single variant martensite (Fig. 5a), some showed a number of crystallographic variants of martensite in the one parent grain (Fig. 5b), and others were characterised by a smooth surface with little apparent relief (Fig. 5c). AFM also revealed that a single parent grain could exhibit a number of small pockets of parallel plates

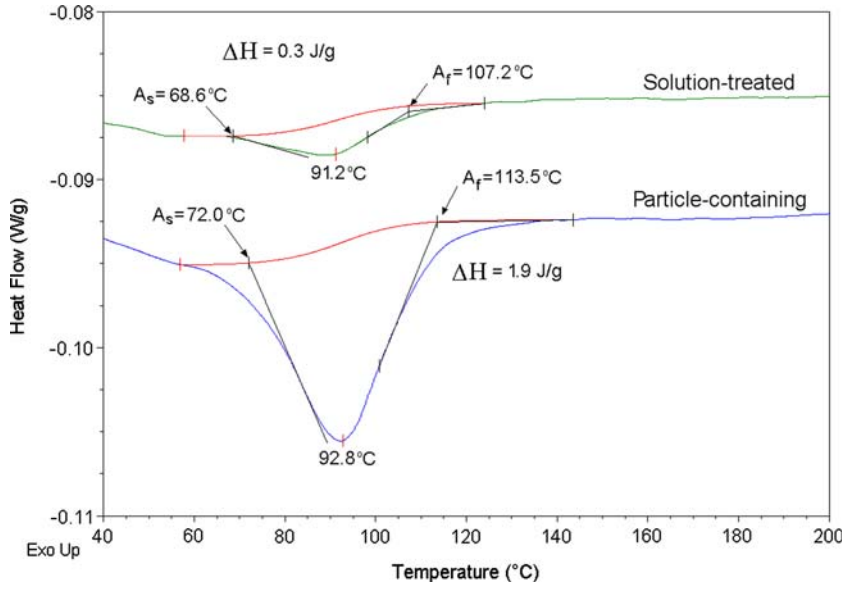

Fig. 2 DSC of heating cycle of solution-treated and particle-containing samples. Exothermic heat flow shown as positive on *y*-axis

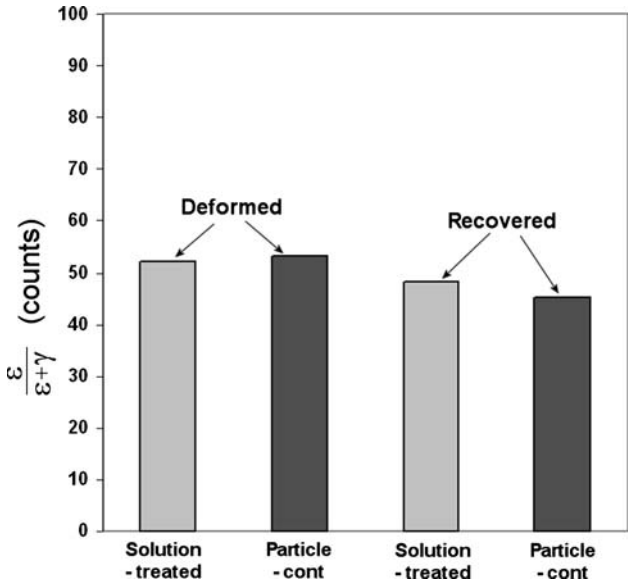

Fig. 3 Relative amount of martensite and austenite determined by X-ray diffraction

(Fig. 5d). This feature was more common on the compressive edges of bent samples.

The AFM images were used to examine the spacing between martensite plates. The average plate spacing was determined using the linear intercept method, but instead of using a straight line as is usually the case, a circle with a circumference of 77 μm was used in each 30×30 μm^2 of microstructure recorded by AFM. The circle was used instead of lines to eliminate the bias arising from plate orientation. This analysis is more fully described in Table 2, and shows that the mean free path between martensite plates in the particle-containing was smaller (1.7 μm) compared to the solution-treated sample (2.2 μm) in the tensile edges. The compressive edges showed a similar plate spacing in both samples (2.1 and 2.2 μm).

Samples deformed by bending to approximately 5% strain were cold mounted, polished and then etched for microstructural analysis. Examples of the microstructure from the tensile region of each sample are shown in Fig. 6a, b. Both the solution-treated and the particle-containing samples showed a mixed microstructure of parent austenite grains containing mostly single variant martensite, or multiple variant martensite, or virtually no martensite. Although the microstructures are similar, the solution-treated sample appeared to have a larger number of grains that were only partially filled with martensite. Another difference between the two samples was that in the high strain regions towards the compressive edge, the particle-containing sample showed a greater concentration of heavily faulted regions with a number of blocky martensite colonies co-existing within a single parent grain (circled in Fig. 6c). These regions also show some plate curvature, indicating that plates formed during bending have been deformed by subsequent ''rotations'' of localised volumes of the parent austenite by plastic deformation.

Microstructure and surface-relief from reversion

Samples deformed by bending to approximately 5% strain were cold mounted to expose the transverse face and then polished flat. The samples were then broken out of the epoxy mount and recovery annealed at 250 °C in a muffle furnace. This temperature is well

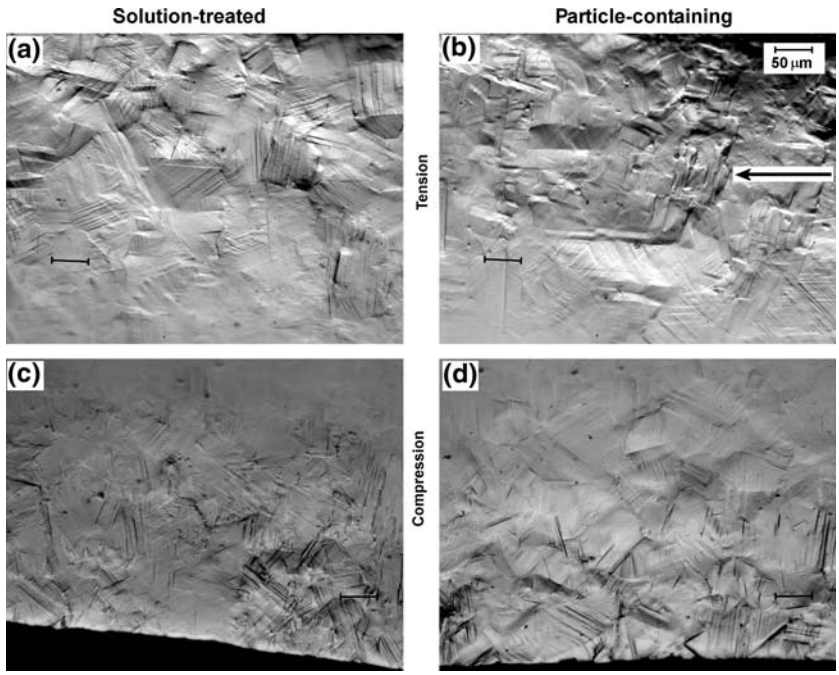

Fig. 4 Optical micrographs of the surface relief produced from deformation by bending in (**a**, **c**) solution-treated condition; (**b**, **d**) precipitation heat-treated condition. The tensile edge is shown in (**a**) and (**b**), and the compressive edge is shown in (**c**) and (**d**). All micrographs taken at the same magnification for a strain of 5% at the outer edge

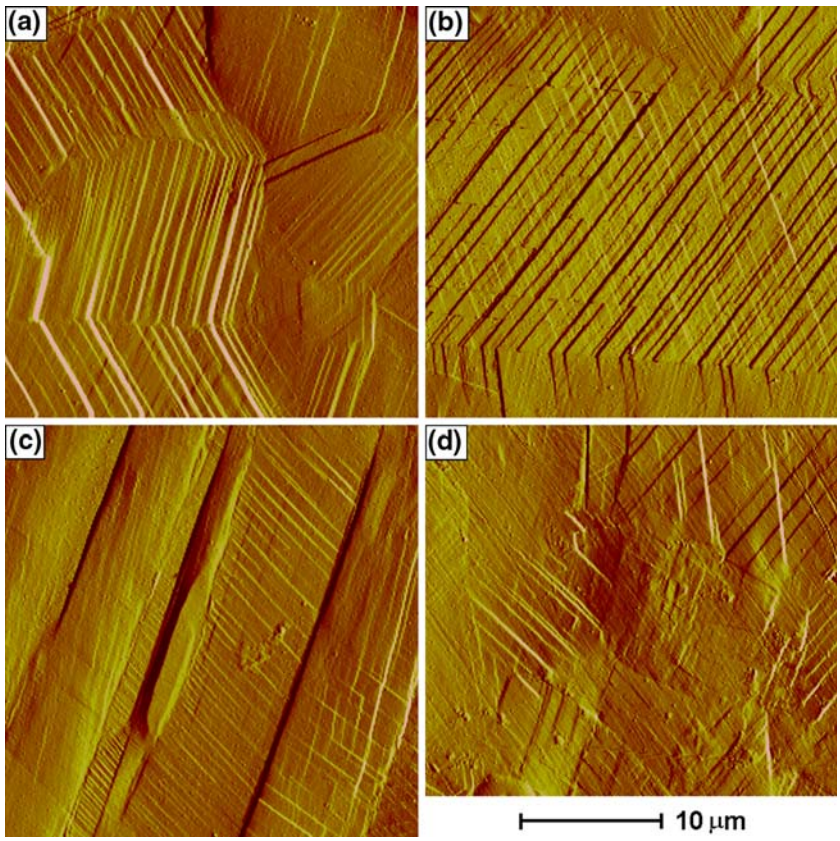

Fig. 5 AFM ''deflection mode'' micrographs of the surface relief produced from deformation by bending. All micrographs taken at the same magnification for a strain of approximately 4%. (**a**) Tensile edge of particle-containing sample. (**b**) Tensile edge of particle containing sample. (**c**) Compressive edge of particle containing sample. (**d**) Compressive edge of solution treated sample

above the ''thermal'' A_f temperature (see Fig. 2). The reversion of martensite to the parent phase austenite causes surface-relief. The surface-relief caused by reversion of martensite was similar in the solution-treated and particle-containing samples (Fig. 7). For both treatments the recovered surface-relief was con-

Table 2 Average spacing between martensite plates determined using the linear intercept method on a circle of 77 μm circumference placed in the centre of AFM images of 30×30 μm^2 in size

Sample		Average spacing	No. areas	SD
Solution-treated	Tension	2.2	5	0.5
	Compression	2.2	5	0.7
Particle-containing	Tension	1.7	4	0.4
	Compression	2.1	5	0.4

The number of images analysed, and the standard deviation of the measurements are also listed

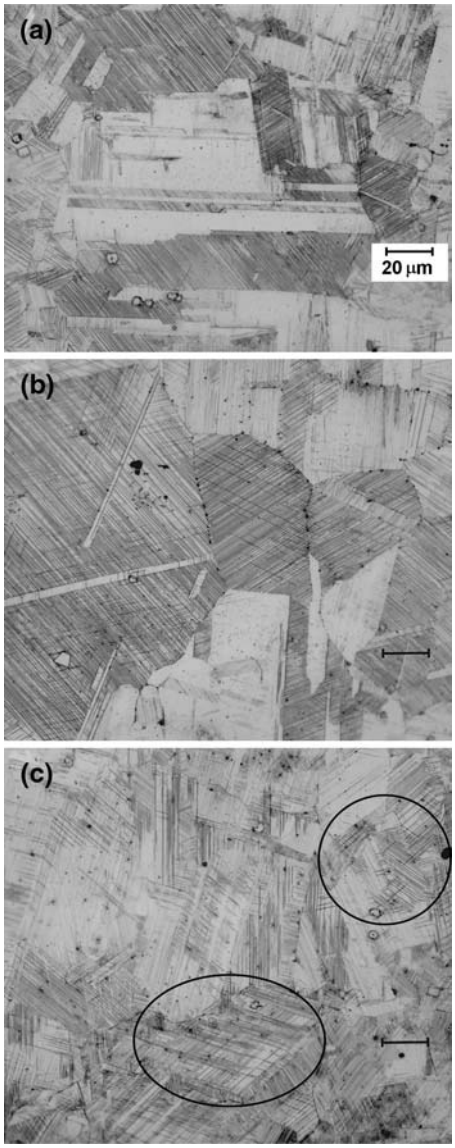

Fig. 6 Optical micrographs of samples deformed in bending by 5%, then polished and etched. (**a**) Solution-treated sample and (**b**, **c**) particle-containing sample. Micrographs (**a**) and (**b**) taken from tensile edge. Micrograph (**c**) taken from compressive edge. All micrographs shown at the same magnification. *Circled* regions show blocky martensite packets, see text for further detail

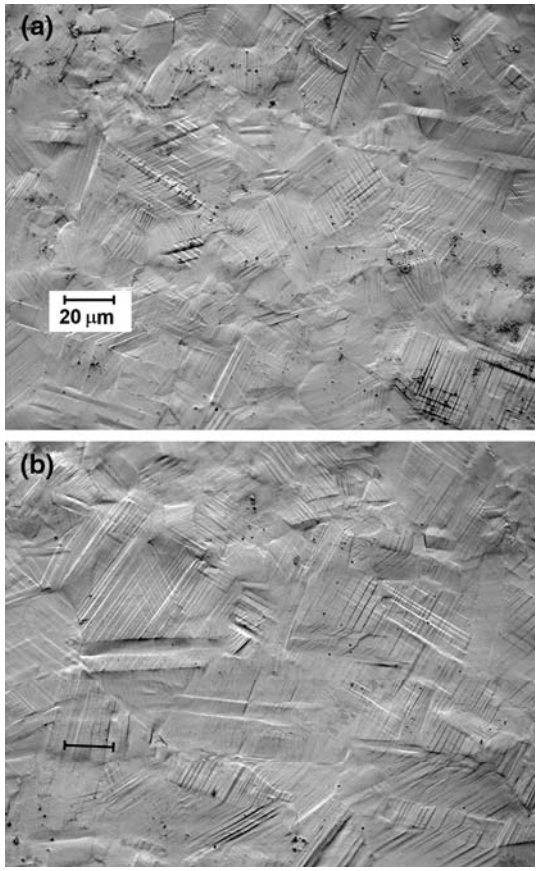

Fig. 7 Parent phase surface relief from reversion of martensite to austenite during recovery annealing in (**a**) solution-treated and (**b**) particle-containing samples. Both micrographs shown at same magnification

sistent with the deformed surface-relief. In the tensile regions, the reverted martensite often revealed the parent grain size. However, this characteristic was much less common in the compressive region. Of particular interest is the number of martensite variants that have reverted within the same volume of microstructure. The most commonly observed number of variants that co-reverted was two, as Fig. 7 clearly shows.

Figure 8 shows AFM recovered surface-relief images from the tensile and compressive regions of both samples. The tensile regions were typified by parallel plate shaped volumes that commonly traversed the whole grain (Fig. 8a), whereas the compressive region (Fig. 8b) consisted of smaller packets of reverted martensite that were often smaller than the parent austenite grain size. AFM did not reveal any significant difference in the recovered surface-relief between the particle-containing and solution treated alloys, except that there appeared to be more reverted plates in the particle-containing sample.

The microstructures after reversion, revealed by polishing and etching, are shown in Fig. 9. As can be seen, a large amount of martensite remains after recovery annealing, particularly in the solution-treated sample. According to Fig. 1, approximately half of the 5% pre-strain is recovered during annealing, resulting in a residual strain of about 2.5%. This residual strain is accounted for by the retained martensite evident in Fig. 9, together with permanent plastic strain in the austenite. The solution-treated sample had more residual martensite than the particle-containing sample, and more grains that contained multiple-variant martensite. In both cases, there was more multiple-variant martensite in the compressive, compared to the tensile region.

TEM

TEM was carried out on a particle-containing sample that had been cold rolled to 5% strain to form stress-induced martensite. The particle-containing samples exhibited precipitates that were present in clusters. The particle size was variable, being between 30 and 300 nm. The particle spacing varied from 0.5 μm within clusters to 5 μm between clusters. Figure 10 shows a cluster of small precipitates and martensite plates. When a deformed sample is thinned for TEM, the reduced volumetric constraint allows some of the stress-induced martensite to revert to austenite. This appears to be the case in the foils prepared, as 5% cold reduction would be expected to show more martensite than was observed. Nonetheless, Fig. 10 does indicate the interaction between particles and martensite plates. There are a number of large particles that are associated with martensite plates, and it appears likely that they influenced the nucleation of these plates.

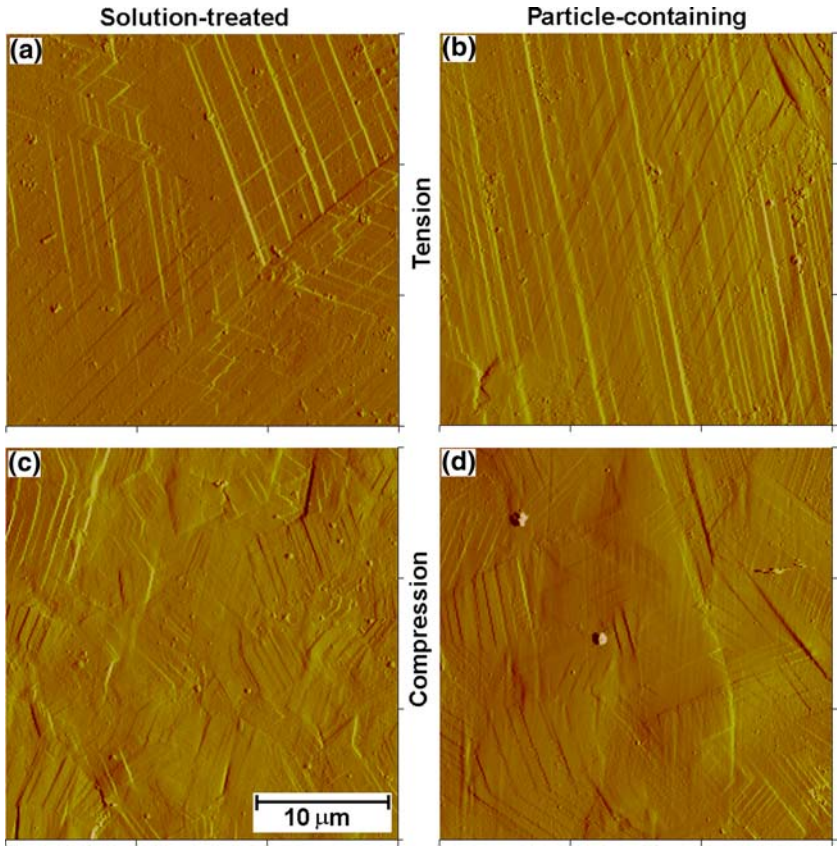

Fig. 8 AFM ''deflection mode'' micrographs of the surface relief produced from reversion of martensite to austenite in (**a**, **c**) solution-treated sample; (**b**, **d**) particle-containing sample. The tensile edge is shown in (**a**) and (**b**), the compressive edge shown in (**c**) and (**d**). All micrographs taken at the same magnification for a bending strain of approximately 4%

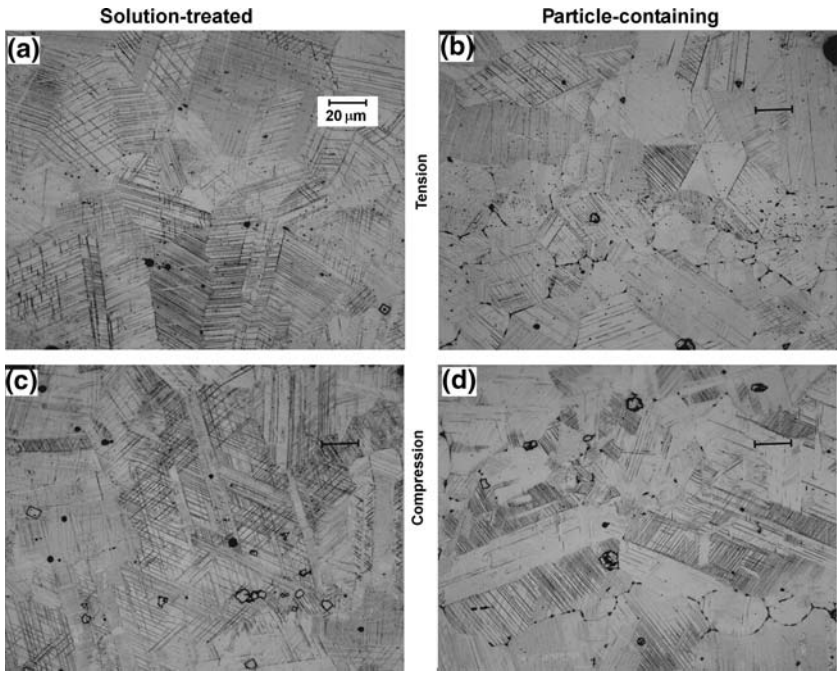

Fig. 9 Optical micrograph of samples deformed 5% by bending and then recovery annealed. All micrographs shown at the same magnification in the polished and etched condition

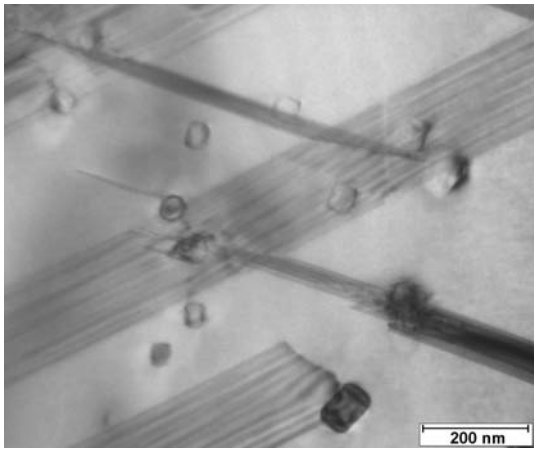

Fig. 10 TEM micrograph of particle-containing sample, cold rolled to 5% strain. The micrograph shown lies in the rolling plane

Discussion

In a previous paper by the authors [5] it was demonstrated that Fe–Mn–Si-based alloys show a tension-compression asymmetry in the surface-relief produced during bending. In the tensile region, large plates span the parent grains producing a surface-relief that reflects the starting parent grain size. This observation is consistent with the features of the tensile edge in Fig. 4a from the solution-treated sample. The tensile region of the particle-containing sample showed similar features in the range of 1–3% tensile strain, exhibiting plate-shaped relief that generally traverses the parent grain. However, at the outer edges, that experienced a tensile strain of about 5%, the microstructure showed more complex domains of relief that were significantly smaller than the grain size (see, for example, the arrowed region in Fig 4b). The more complex features exhibited by the particle-containing sample at higher strains could be caused by a greater incidence of plastic deformation that is manifest in tilting/upheaval of the surface. However, the microstructure revealed by polishing and etching suggests that the more complex relief is associated with the activation of different variants of martensite within partitioned regions of a parent austenite grain. This feature is shown in the circled regions of the polished and etched microstructure in Fig. 6c, and is also evident in a number of the surface-relief micrographs such as Fig. 4b. The observation that colonies of parallel martensite plates are able to form in volumes that are much smaller than the parent grains also explains the ''subgrain'' appearance of some of the surface-relief micrographs in compressive regions. For example, Fig. 5c shows packets of martensite that lie within regions that are smaller than the parent grain. A possible explanation for the presence of these smaller packets of martensite is that they form in austenite that has been partitioned by other martensite plates or by deformation bands. It is proposed that their frequency is higher in the particle-containing sample because of the nucleating sites provided by the particles.

Observations of the microstructure of regions in both samples deformed up to 3% strain showed there

were grains that did not appear to have a significant amount of stress-induced martensite, presumably because they are unfavourably oriented with respect to the applied stress. For higher strains, these martensite-free regions are likely to be activated in the particle-containing sample by particle-enhanced nucleation of martensite. However, in the solution-treated sample these regions are more likely to remain un-transformed and to undergo strain by irreversible plastic deformation.

Although it has been suggested [6] that formation of one variant only within the parent grain is a critical criterion for reversion back to parent phase, the representative surface-relief features of Figs. 7 and 8 indicate that this is rarely the case. Although much of the reversion topography is dominated by a single martensite variant, closer inspection of these regions usually reveals that a second variant with larger plate spacing is often present, e.g. Fig. 8a, b. Furthermore, Fig. 9 shows that the martensite remaining in the microstructure that did not revert during recovery annealing is often single variant, particularly in the case of the particle-containing alloy. If single variant formation was the only criterion for reversion then these regions would be expected to revert to austenite, and the only remaining martensite would in this case be multiple variant clusters.

Many of the martensite plates remaining in Fig. 9 are aligned at ~45° to the tensile direction. This observation could explain why these regions and not others were unable to transform back to austenite. It is possible that the grains exhibiting retained martensite were subjected to plastic deformation by slip during or after the formation of the stress-induced martensite. The slip system for fcc austenite is $\{111\}\langle 110\rangle$ [7] and since the shear stress will be a maximum on {111} planes inclined at 45° to the tensile axis [7], both slip and the formation of martensite will be favoured on these planes. If martensite forms on the same {111} planes that undergo deformation by slip, residual dislocation loops are likely to be present that can pin the interface between martensite and austenite, degrading the capacity of martensite to revert to austenite. Although slip is likely to inhibit martensite reversion regardless of the orientation of the martensite variant, it is likely to be more intense and effective on planes close to ±45° to the surface.

The martensite plates produced in the solution-treated samples in response to bending tended to span the parent grain and then stop growing, see, for example, the relief features in Fig. 4a. In the particle-containing samples, martensite can be nucleated at particles as demonstrated by Fig. 10. Increased pre-strain results in nucleation of new martensite plates at particles between those plates that have already formed. This argument is consistent with the AFM observations of finer plate spacing in the particle-containing sample, and also with the smaller features shown in Fig. 4b. These extra plates grow to consume a larger portion of the austenite grain than would be possible in the absence of particles. The existence of this extra martensite in the particle-containing samples is also consistent with the DSC results that show a much larger austenite reversion peak in the particle-containing sample compared to the solution-treated sample, indicating reversion of a greater volume fraction of martensite. It is also consistent with the XRD results that show a larger portion of martensite in the particle-containing, compared to the solution-treated samples.

It is evident that the increased SME exhibited by alloys that contain second phase particles is primarily a result of these particles acting as nucleation sites for the formation of martensite. It is inferred that the hard second-phase particles can act as stress concentrators in the matrix during pre-strain, generating stacking faults (SF) that provide nuclei for martensite formation. The presence of relatively coarse, incoherent particles provides a weak alternative to thermal-mechanical training. Successive deformation and recovery annealing cycles are known to establish a high density of SF nuclei for formation of stress-induced martensite [8]. It is proposed that during pre-strain, the particles provide an alternative means of stimulating martensite nucleation by generating SF nuclei in zones of enhanced deformation around the particles. Even without strain-induced faulting in the austenite surrounding the particles, a volumetric strain would be expected on quenching due to differential thermal contraction between particles and matrix, leading to dislocation generation around the particles. As a result, the proportion of thermal martensite formed on cooling to a given sub-zero temperature would be expected to be higher for the particle-containing sample. This hypothesis is supported by the DSC data for the enthalpy of martensite reversion (see Fig. 2).

The change in martensite surface-relief found in the presence of particles, and the change in transformation behaviour measured using DSC and XRD provide evidence to support the hypothesis that the particles act as nucleants for martensite formation. These results suggest that, for a given pre-strain, the formation of a greater fraction of martensite, rather than more efficient reversion, is the main cause of improved SME in particle-containing alloys. More of the ''deformation'' process takes place by a potentially reversible mechanism

(reversion of stress-induced martensite), compared with the same alloy in the solution-treated condition. Particles aid in the formation of additional, and more finely spaced plates during the initial stages of deformation. With further deformation, in those regions that are not ideally oriented for the formation of martensite, the particle-containing alloy is able to form small packets of martensite between previously formed plates to produce small features such as shown in Fig. 4b. These small packets of martensite extend the potentially reversible strain due to the martensite shape change, and thereby inhibit permanent plastic deformation. The activation of different variants within an individual parent austenite grain is a key factor that increases the amount of stress-induced martensite compared to the solution-treated case.

Conclusions

The following conclusions were drawn from comparisons of the shape memory performance, the capacity to form martensite under bending stress and the characteristics of the reverse transformation on heating.

(i) Shape memory

- The presence of moderately large TiC precipitates increases the percent recovery of 5% pre-strain from 44% in the solution-treated sample to 54% in the particle containing sample.

(ii) Martensite formation under bending stress

- Optical microscopy and observations of the surface-relief formed by deformation showed that the particle-containing alloy exhibited martensite in more grains, and had more finely spaced martensite with more complex surface relief features compared to the solution-treated sample.
- The microscopical observations are consistent with the formation of a higher proportion of stress-induced martensite in the case of the particle-containing sample.
- The transformational heat flow measured by DSC indicated that more thermal martensite was also produced in the particle-containing alloy.
- X-ray diffraction showed that more stress-induced martensite is formed during cold rolling of the particle-containing compared to the solution-treated samples.

(iii) Martensite reversion on heating

- Optical microscopy showed that more unreverted martensite remained in the solution-treated samples. This retained martensite was often aligned at ±45° to the tensile axis. It is suggested that slip on these systems during or after the formation of martensite hinders reversion to parent phase during recovery annealing.
- AFM and optical microscopy of surface-relief after recovery annealed showed that the reversion of martensite to parent phase was generally similar in the particle-containing and solution-treated samples. In both cases, the surface-relief due to reversion typically showed two or more variants co-reverting within the same volume of microstructure.

Acknowledgements The research described in this paper was funded by the Australian Research Council *Discovery Grant* scheme. The authors would also like to thank Mr. Greg Tillman for his assistance with AFM.

References

1. Kajiwara S, Liu D, Kikuchi T, Shinya N (2001) Scripta Mater 44:2809
2. Baruj A, Kikuchi T, Kajiwara S, Shinya N (2003) J Phys IV 112:373
3. Dong Z, Liu W, Chen J, Wang D (2003) J Phys IV 112:389
4. Stanford N, Dunne DP (2006) J Mater Sci 41(15):4883
5. Stanford N, Dunne D (2005) Scripta Mater 53:739
6. Liu DZ, Kajiwara S, Kikuchi T, Shinya N (2003) Phil Mag 83:2875
7. Deiter GE (1988) Mechanical metallurgy, Metric edition. McGraw Hill Book Co
8. Otsuka H, Murakami M, Matsuda S (1989) In: Doyama M, Sōmiya S, Chang R (eds) Proceedings of the MRS international meeting on advanced materials, vol 9, Tokyo, Japan 1998, Materials Research Society, Pittsburgh, p 451